01 Jan 2007

Determination of Laser Absorption Coefficients of Gas Mixtures using an Ab Initio Md Model

Zhi Liang
Missouri University of Science and Technology, zlch5@mst.edu

Hai-Lung Tsai
Missouri University of Science and Technology, tsai@mst.edu

Lan Jiang

Recommended Citation

Z. Liang et al., "Determination of Laser Absorption Coefficients of Gas Mixtures using an Ab Initio Md Model," *ASME International Mechanical Engineering Congress and Exposition, Proceedings (IMECE)*, vol. 8, pp. 1013 - 1019, American Society of Mechanical Engineers (ASME), Jan 2007.
The definitive version is available at https://doi.org/10.1115/IMECE2007-41449

Proceedings of IMECE2007
2007 ASME International Mechanical Engineering Congress and Exposition
November 11-15, 2007, Seattle, Washington, USA

IMECE2007-41449

DETERMINATION OF LASER ABSORPTION COEFFICIENTS OF GAS MIXTURES USING AN AB INITIO MD MODEL

Zhi Liang, Hai-Lung Tsai*
Laser-Based Manufacturing Laboratory
Department of Mechanical and Aerospace Engineering
University of Missouri-Rolla, Rolla, MO 65409

Lan Jiang
Department of Mechanical and Automation Engineering,
3rd School
Beijing Institute of Technology, 100081, P.R. China

ABSTRACT

In an effort to study the laser induced dissociation of gas mixtures for an ongoing research project on diamond thin film coating using multiple lasers, it is necessary to determine the absorption coefficient of laser energy by CO_2 gas. An ab initio molecular dynamics (AIMD) model is used to determine the laser absorption coefficient of CO_2 gas as a function of laser wavelength and gas temperature. The translational, rotational, and vibration motions of molecules are all taken into account in our model. The intra-molecular potential energy is obtained by solving the Kohn-Sham equation. The Projector-Augmented Wave (PAW) exchange-correlation potential function is used in the ab initio calculation. Specific heat of the CO_2 gas is also calculated. The calculated thermal properties of CO_2 gas and the vibration spectrum of molecules are in good agreement with the experimental results. The calculated normalized absorption line shape CO_2 gas is close to the experimental results.

INTRODUCTION

Multiple laser beams diamond coating techniques demonstrate unique advantages over conventional PVD or CVD methods [1-7]. In a reported high-speed multiple laser coating process [5-7], a diamond or diamond-like carbon film was formed in which CO_2 gas is used as the sole precursor or secondary precursor. Though the phenomenon was found in the experiments, the fundamental mechanisms involved in the process are not well understood [1,5-10].

To study the laser matter interaction, an AIMD model is used in our calculations. One of the important problems in AIMD is to determine the intra-molecular potential energies. In our model, these potential energies are obtained by solving many-electron Schrödinger equations. Due to the antisymmetric property of electronic wave functions and interactions between different electron energy states, the exchange-correlation potentials exist in a many-electron system. The Projector-Augmented Wave (PAW) exchange-correlation potential function is chosen in our calculations. By solving the electronic Schrödinger equations, we get intra-molecular potential energies as well as dipole moments as a function of nuclear configuration.

The calculated potential energies are used in a molecular dynamics model to calculate the thermodynamic properties of CO_2 gas. The results are compared with the experimental data to assure the calculated potential energies are valid.

The absorption coefficient of a gas is related to the time correlation function of the molecular dipole moment [11,12]. A CO_2 molecule has no permanent dipole moment. The oscillating dipole moment is produced by its asymmetric stretch and bending vibration modes. To calculate the transitional dipole moment, nuclear Schrödinger equations must be solved. The potential energies used in the equations are the ones obtained from the electronic Schrödinger equations mentioned above.

In the following sections, we amplify these introductory remarks, and then show the results.

NOMENCLATURE

$\hat{H}$	=	Hamiltonian operator
R	=	nuclear coordinates
x	=	electron coordinates
T_N	=	nuclear kinetic energy operator
T_e	=	electron kinetic energy operator
V_{ee}	=	electron repulsive potential
V_{NN}	=	nuclear repulsive potential
V_{eN}	=	electron-nuclear attractive potential
J	=	rotational state quantum number
$N(E_J)$	=	energy distribution
E_J	=	energy of rotational quantum states
$G(J)$	=	degeneracy of energy level J
C_V	=	heat capacity
$\bar{\mu}$	=	electric dipole moment
E_0	=	the amplitude of electric field

* Corresponding Author: Tel: +1-573-341-4945; Fax: +1-573-341-4607; Email address: tsai@umr.edu.

$|i\rangle$ = initial quantum state

$|j\rangle$ = final quantum state

$E_{i,j}$ = energy eigen values for rotation-vibration motion of molecules

$\vec{u}$ = unit vector along the direction of the transition dipole moment

Greek Symbols

Φ = electron-ion system wave function

Ψ = electron wave function

χ = nuclear wave function

ε = energy eigen value

$\vec{\varepsilon}$ = unit vector along the electric field

$\vec{l}$ = lattice vector of cubic box

$\vec{K}$ = wave vector

$\alpha(\vec{K})$ = coefficient of basis set

ρ_i = Boltzmann factor for the initial rotation-vibration state

ANALYSIS

The intra-molecular dynamics, i.e. rotational and vibration motions, of molecules play a critical role in laser-gas interactions. The intra-molecular dynamics are determined by the following Schrödinger equations for an electron-ion system:

$$\hat{H}\Phi(x,\vec{R}) = \varepsilon(x,\vec{R})\Phi(x,\vec{R}) \tag{1}$$

where $\hat{H} = \hat{T}_N + \hat{T}_e + V_{ee}(\vec{r}) + V_{NN}(\vec{R}) + V_{eN}(\vec{r},\vec{R})$

Equation (1) is too complex to be solved directly. Using a highly accurate and simplifying approximation – Born-Oppenheimer (BO) approximation, the electronic motion and the nuclear motion in molecules can be separated [13],

$$\Phi(x,\vec{R}) = \Psi(x,\vec{R})\chi(\vec{R}) \tag{2}$$

and equation (1) can be separated adiabatically into two coupled Schrödinger equations: a many-electron Schrödinger equation (3) and a nuclear Schrödinger equation (4).

$$\left[\hat{T}_e + V_{ee}(\vec{r}) + V_{eN}(\vec{r},\vec{R})\right]\Psi(x,\vec{R}) = \varepsilon(\vec{R})\Psi(x,\vec{R}) \tag{3}$$

$$\left[\hat{T}_N + V_{NN}(\vec{R}) + \varepsilon(\vec{R})\right]\chi(\vec{R}) = E\chi(\vec{R}) \tag{4}$$

The electronic potential energies ε(R) obtained from equation (3) will be used in equation (4).

The wave function Ψ in a many-electron Schrödinger equation (3) must fulfill anti-symmetric property since electrons are fermions. This property leads to the use of Slater determinants as the basis functions of the electron wave function, which is too complex to be implemented. To solve this problem, Density Functional Theory (DFT) is used. Using DFT, the many-electron Schrödinger equation could be transformed to an effective one electron Schrödinger equation (i.e., Kohn-Sham equation) as

$$\hat{H}^{KS}\psi_i^{KS}(1) = \varepsilon_i^{KS}\psi_i^{KS}(1) \tag{5}$$

where $\hat{H}^{KS} = \underbrace{-\frac{1}{2}\nabla_1^2}_{\text{kinetic energy of electrons}} \underbrace{-\sum_A \frac{Z_A}{\vec{r}_{iA}} + \int \frac{\rho(\vec{r}_2)}{r_{12}} d\vec{r}_2 + v_{xc}(1)}_{V_{eff}(\vec{r})}$

In equation (5), $\psi^{KS}(1)$ is one electron wave function and $\rho = \sum_{i=1}^{n} |\psi_i^{KS}|^2$ is electron charge density. Equation (5), i.e., the KS equation is written in atomic units. The Hamiltonian in KS equation contains 4 components. The first one is the electron kinetic energy. The remaining three are the effective one electron potential. The first two potentials have semi classical interpretations, i.e., electron-nuclear attraction potential and electron-electron repulsive potential. The last potential is the exchange-correlation potential of electrons v_{xc}. This potential is not found in the Hamiltonian of equation (3). It is caused by anti-symmetric property of many-electron wave functions and electron configuration interactions. It does not have semi classical interpretations.

If v_{xc} is known, the Hamiltonian $\hat{H}^{KS}$ can be easily found. To solve the KS equation, we need to construct ψ^{KS} with basis functions as follows:

$$\psi_i = \sum_{\mu=1}^{K} C_{\mu i}\phi_\mu \quad i = 1,2,\ldots K \tag{6}$$

where ϕ_u are known as the basis functions. Using equation (6) in equation (5) and dot multiplying ϕ_u on both sides of the KS equation, we can get the following K×K matrix equation.

$$HC = SC\varepsilon \tag{7}$$

where H is the KS Hamiltonian matrix:

$$H_{\mu\nu} = \int d\vec{r}_1 \phi_\mu^*(1)\hat{H}^{KS}(1)\phi_\nu(1)$$

and S is the basis function overlap matrix:

$$S_{\mu\nu} = \int d\vec{r}_1 \phi_\mu^*(1)\phi_\nu(1)$$

The coefficients $C_{\mu i}$ in equation (6) and the eigen values ε_i are determined by solving equation (7).

Two problems exist in solving the KS equation; one is the unknown exchange-correlation potential v_{xc} and the other is the choice of basis functions. We will discuss the selection of basis functions in the next section.

Since v_{xc} is unknown, some approximations must be made to obtain appropriate v_{xc}. In our calculations, we used a PAW v_{xc} which is supplied by the Vienna *Ab Initio* Simulation Package (VASP). In VASP, plane wave (PW) basis functions are chosen. VASP calculates the electronic ground state self-consistently at each molecular configuration. We use this software to calculate the intra-molecular potential energy and dipole moment. These results are used as the data base for later calculations.

RESULTS AND DISCUSSION

CO_2 molecule in a cubic box

In the first step, we calculate the intra-molecular potential ε(R) in equation (3) which will be used in equation (4).

At each nuclear configuration, the nuclear coordinates {R} are fixed. We choose PAW exchange-correlation potentials of carbon atom and oxygen atom to setup the Hamiltonian of KS equation H^{KS}. By solving equation (7) the total potential energy ε({R}) is determined.

In the calculation, the CO_2 molecule is placed in a cubic box with length L. Periodic Boundary Conditions (PBC's) are applied. Compatible with PBC's, PW functions are chosen as the basis sets.

$$\psi(\vec{r}) = \sum_{\vec{K}} \alpha(\vec{K}) e^{i\vec{K}\cdot\vec{r}} \text{ where } \vec{K}\cdot\vec{l} = 2\pi m,\ m \text{ intergers} \tag{8}$$

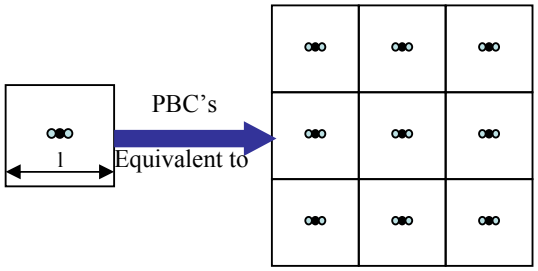

Fig. 1 CO_2 in a cubic box with PBC's

The PW functions have a big advantage in solving KS equations because the Hamiltonian matrix elements in equation (7) now becomes $\hat{H}_{\vec{K}'\vec{K}} = \frac{1}{V}\int d\vec{r}_1 \left(e^{i\vec{K}'\cdot\vec{r}}\right)^* \hat{H}^{KS}(1) e^{i\vec{K}\cdot\vec{r}}$. In equation (5), we know $\hat{H}^{KS} = -\frac{1}{2}\nabla_1^2 + V_{eff}(\vec{r})$. So

$$\begin{aligned}\hat{H}_{\vec{K}'\vec{K}} &= \frac{1}{V}\int \left(e^{i\vec{K}'\cdot\vec{r}}\right)^* \left(-\tfrac{1}{2}\nabla^2 + V_{eff}\right) e^{i\vec{K}\cdot\vec{r}}\, d\vec{r} \\ &= \frac{\vec{K}^2}{2}\delta_{\vec{K}\vec{K}'} + \underbrace{\frac{1}{V}\int V_{eff} e^{i(\vec{K}-\vec{K}')\cdot\vec{r}}\, d\vec{r}}_{\text{Fourier transform of } V_{eff}}\end{aligned} \tag{9}$$

One can see that the second part of the Hamiltonian matrix elements is the Fourier transform of an effective potential which can be easily evaluated.

Although the PBC's with PW basis sets could save much computational time, this method brings one problem. As shown in Fig. 1, there exist spurious interactions of aperiodic charge density with its images in the neighboring boxes. The potential energy E(L) calculated in a finite cubic box with length L differs from the potential energy calculated in the limit $E_0 = E(L\to\infty)$. To estimate E_0 from the calculated E(L), we need to know the asymptotic dependence of E on L. It was proved [14] that the asymptotic behavior of an isolated neutral molecule in a cubic box can be determined by the quadrupole-quadrupole interaction, which has a functional dependence of L^{-5}.

$$E(L) = E_0 + O(L^{-5}) \tag{10}$$

To get the appropriate box size we calculated the equilibrium configuration of CO_2 and the energy required to stretch a C=O bond 0.05Å off the equilibrium position as a function of box size, which is shown in Fig. 2. The cutoff energy of PW basis functions are set to be 500 eV.

From the simulation, at equilibrium configuration, the three atoms in the CO_2 molecule are collinear; C is in the center of two O atoms. From Fig.2 we can see both the bond length and the stretching energy converge rapidly with box size. Although more accurate results could be obtained by using a larger box size, the computational time increases tremendously. Box size of 10Å is a good choice for CO_2 potential energy calculations. At this box size, the C=O bond length and the CO_2 molecule rotational constant are calculated and compared with experimental values [15] which are shown in Table 1.

Table 1. Constants of linear molecule CO_2

bond length (Å)		rotational constant (cm^{-1})	
ab initio	experiment	ab initio	Experiment
1.168	1.162	0.384	0.39

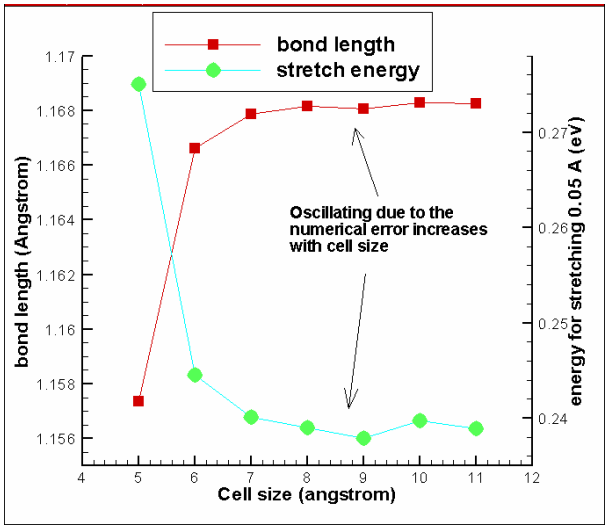

Fig. 2 C=O bond length and stretching energy vs. box size

Using this cubic box we made a table of CO_2 intra-molecular potential energies at different nuclear configurations. Three coordinates are enough to describe one CO_2 molecular configuration. This result will be used in the calculation of the CO_2 vibration spectrum which is shown in the next section. The dipole moment is also calculated as a function of nuclear configurations which will be used in the calculation of the absorption coefficient.

CO_2 molar heat capacity

From the above results we can see CO_2 is a polyatomic linear molecule. Hence, the heat capacity of CO_2 gas contains three parts.

- Translational heat capacity, $C_{v,t}$
- Rotational heat capacity, $C_{v,r}$
- Vibration heat capacity, $C_{v,v}$

Assuming the translational, rotational and vibration motions of molecules in the gas are separable, we calculate the three parts of heat capacity, respectively.

If the weak interactions between molecules are neglected, the translational heat capacity of CO_2 gas is $C_{v,t} = 3k_B/2$ since the translational motion has 3 degrees of freedom. This result is proved by the equipartition theorem.

The rotational and vibration heat capacities do not have the above simple relation because of the quantum effects of rotational and vibration motions of CO_2 molecules.

The rotational motion of a CO_2 molecule can be modeled as a quantum rigid rotor. The exact solution of the rigid rotor Schrödinger equation exists. The rotational energy distribution fulfills the following Boltzmann distribution.

$$N(E_J) \propto G(J) e^{-\frac{E_J}{k_B T}} \quad J = 0,1,2,\cdots \tag{11}$$

where $E(J) = -\frac{J(J+1)\hbar^2}{2I\,(k_B T)}$ and $G(J) = 2J+1$

E(J) and G(J) are the solutions of the rigid rotor Schrödinger equation.

Rotational energy E(J) depends on the CO_2 moment of inertia I. The value of I can be obtained from the simulations shown in the first step which is equal

to $7.2904\times10^{-46}\ \mathrm{kg\cdot m^2}$. The average energy and heat capacity are both a function of temperature, and they are:

$$\langle E\rangle_T = \frac{\sum_{J=0}^{\infty}\frac{J(J+1)\hbar^2}{2I}(2J+1)\exp\left(-\frac{J(J+1)\hbar^2}{2I(k_BT)}\right)}{\sum_{J=0}^{\infty}(2J+1)\exp\left(-\frac{J(J+1)\hbar^2}{2I(k_BT)}\right)} \qquad (12)$$

and $C_V = \frac{\partial\langle E\rangle}{\partial T}$

The results are shown in Fig. 3.

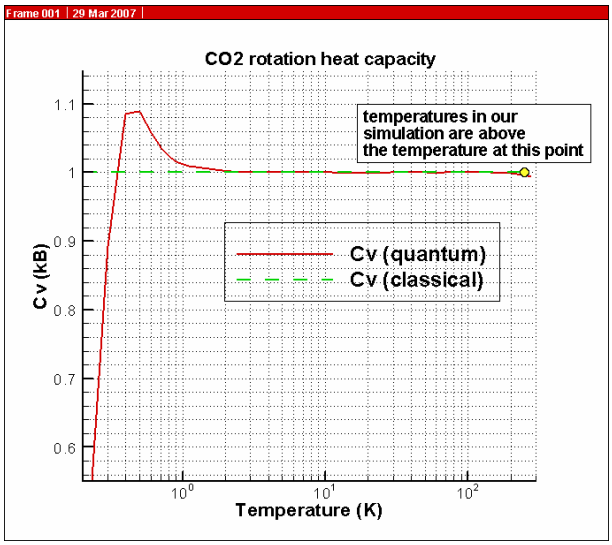

Fig. 3 CO_2 rotational heat capacity vs. temperature

In classical mechanics, the heat capacity of a rigid rotor is exactly $1k_B$ because its motion has two degrees of freedom. From Fig. 3 we can see that the quantum mechanics result only differs from the classical mechanics result at very low temperatures. The temperature of CO_2 gas is usually higher than $\sim10^2$K. At this range of temperature, the quantum effect of rotational motion can be neglected. So the rotational heat capacity of CO_2 gas is $C_{v,r}= 1k_B$, a constant. The results are reasonable because the rotational energy gaps between neighboring levels are quite small ($\sim10\mathrm{cm}^{-1}$) compared to the temperature at $\sim10^2$K ($k_BT\sim10^2\mathrm{cm}^{-1}$).

The vibration energy and heat capacity depends on the solution of the CO_2 vibration Schrödinger equation. Since CO_2 has three atoms, there is no analytical solution of its Schrödinger equation. When temperatures are not high ($\sim10^2$K), we approximate the intra-molecular potential as a harmonic potential so that we can use the solutions of the harmonic oscillator Schrödinger equation in our calculations.

A good property of the quantum harmonic oscillator is the energies on different energy levels depend on the frequency ω of the corresponding classical harmonic oscillator. The energy function can be expressed as

$$E_n = \left(n+\tfrac{1}{2}\right)\hbar\omega \quad n=0,1,2,\cdots \qquad (13)$$

As a linear molecule, CO_2 has 3n − 5 = 4 vibration modes, where n is the number of atoms in the molecule. To determine the frequencies of these different vibration modes, we stretch the atoms in the molecule a little bit from their equilibrium positions and let it go. The initial velocities of atoms are all set to be zero. The force acting on each atom in the molecule can be calculated from the potential table. Using classical MD simulation, we can get the atomic positions as a function of time r(t). The Fourier transform of this function is the molecular vibration spectrum in classical mechanics as follows:

$$g(\omega) = \int r(t)\, e^{-i\omega t}dt \qquad (14)$$

The results are shown in Fig. 4.

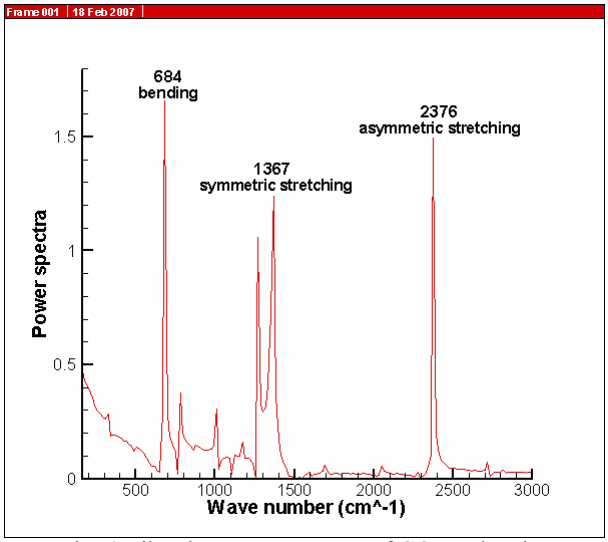

Fig. 4 Vibration power spectra of CO_2 molecules

A CO_2 molecule has 4 vibration modes. In figure 4, we only find 3 vibration modes. This is because the bending mode is doubly degenerated. The results are very close to the experimental values [16] which are shown in Table 2.

Table 2. Vibration spectrum of CO_2

Vibration mode	ω(cm^{-1}) calculated	ω(cm^{-1}) experimental
Bending	684	667
Symmetric stretch	1367	1388
Asymmetric stretch	2376	2349

The average vibration energy and heat capacity of each vibration mode are both a function of temperature, and they can be written as follows:

$$\langle E\rangle_T = \tfrac{1}{2}\hbar\omega + \frac{\hbar\omega}{\exp(\hbar\omega/k_BT)-1} \text{ and } C_V = \frac{\partial\langle E\rangle}{\partial T} \qquad (15)$$

In equation (15), $\hbar\omega$ is the vibration energy gap. The values of energy gaps can be found in Table 2.

$$C_{V,v} = \sum_n C_{V,v_n} \text{ where n is the mode number} \qquad (16)$$

The result is shown in Fig. 5. The dashed line in Fig. 5 is the vibration heat capacity in classical mechanics. In classical mechanics, each vibration mode has a $1k_B$ heat capacity. Hence, the total vibration heat capacity is 4 k_B for CO_2 molecules. From Fig. 5, we can see the CO_2 vibration motions have a very strong quantum effect even at $\sim10^3$K. The quantum mechanics results are much lower than the classical results at room temperature. Apparently, the classical approximation is not valid here. We cannot use classical MD simulation to study the dynamics of CO_2 vibration.

Using the above result, we find the vibration heat capacity of CO_2 gas $C_{v,v}$ (T = 288.15K) = 0.905k_B. Combining with the former results, $C_v = C_{v,t}+C_{v,r}+C_{v,v}$ = 3.405k_B at 288.15K. This result is very close to the experimental value 3.40k_B at 288.15K and 1atm.

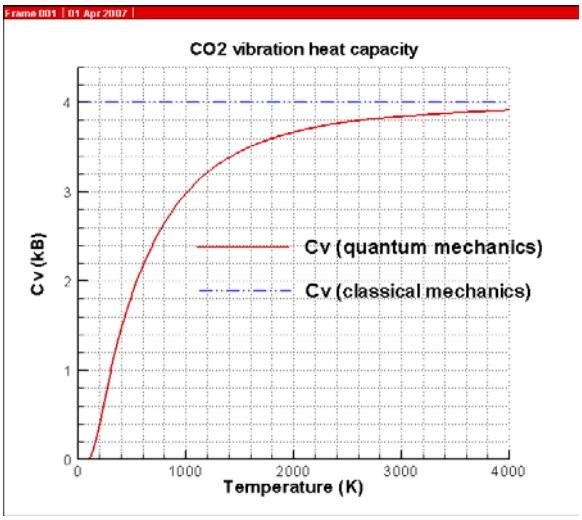

Fig. 5 CO_2 vibration heat capacity vs. temperature

Absorption coefficient of CO_2 gas

When molecules in the gas interact with an electric field of frequency ω, the interaction between the field and the molecules can be written as

$$\hat{H}^{(1)} = -\vec{\mu}\cdot\vec{E}(t) \tag{17}$$

If we let the field be monochromatic, then we can write

$$\vec{E}(t) = E_0\vec{\varepsilon}\cos(\omega t) \tag{18}$$

According to Gordon [11], the expression for an absorption band shape, in terms of transitions between quantum states, is

$$I(\omega) = \sum_{ij}\rho_i\left|\langle f|\vec{\varepsilon}\cdot\vec{\mu}^v|i\rangle\right|^2\delta\left[\left(E_j-E_i\right)/\hbar-\omega\right] = \frac{1}{2\pi}\int_{-\infty}^{+\infty}e^{-i\omega t}\,\tfrac{1}{3}\left\langle\vec{\mu}^v(0)\cdot\vec{\mu}^v(t)\right\rangle dt \tag{19}$$

Equation (19) expresses the Heisenberg-type description of an infrared band shape. The distribution of absorption frequencies about the vibration frequency is the Fourier transform of the average motion of the transition dipole moment [11].

The normalized absorption line shape function is

$$\hat{I}(\omega) = \frac{1}{2\pi}\int_{-\infty}^{+\infty}e^{-i\omega t}\left\langle\vec{u}(0)\cdot\vec{u}(t)\right\rangle dt \tag{20}$$

Hence, the key to determine the absorption coefficient is to obtain the time correlation function $\left\langle\vec{u}(0)\cdot\vec{u}(t)\right\rangle$. This correlation function is related to the thermal motion of molecules.

A CO_2 molecule has no permanent dipole moment. However, the anti-symmetric stretch and the bending vibration mode produce oscillating dipoles. The dipole moment in the first case oscillates along the axis of the molecule, and the dipole moment in the second case oscillates perpendicular to the axis. The oscillating frequency is determined by the corresponding vibration band as the result shown in Table 2. In this case the frequency ω in equation (20) is replaced by $\omega_0+\omega$, where ω_0 is the vibration band center.

An MD model is used to calculate the correlation function. The CO_2 molecule is considered as a linear rigid molecule. A Lennard-Jones potential is used to calculate the interaction between molecules. The parameters we used in the simulation are shown in Table 3. Interactions between unlike atoms are approximated using the venerable Lorentz-Berthelot mixing rules.

Table 3. Interaction parameters

Atom	ε/k_B (K)	σ (Å)
C	51.2	3.35
O	61.6	2.95

An NVT ensemble is used in the simulation, and 4096 molecules are included. The translational and rotational velocities are initialized according to the Boltzmann distribution at the simulation temperature. A leap frog algorithm is used to integrate the equations of motion. At each time step, the direction of the molecular vibrating dipole $\vec{u}(t)$ is measured. Note $\left\langle\vec{u}(0)\cdot\vec{u}(t)\right\rangle$ is the project of $\vec{u}(t)$ on the initial direction. Fig. 6 is a snapshot of CO_2 gas at thermal equilibrium.

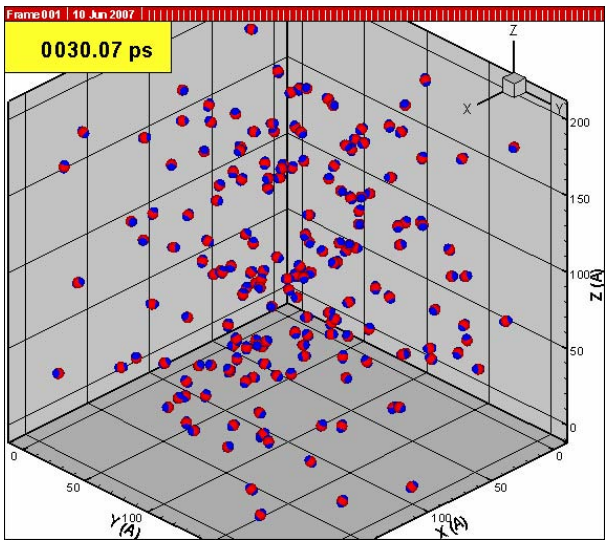

Fig. 6 A snapshot of CO_2 gas

The first 1ns computation time is used for equilibrating the system. The distributions of translational and rotational kinetic energies are measured and compared with theoretical results which are shown in Fig. 7 and Fig. 8, respectively. The system is simulated at 300K and 1atm.

From Fig. 7 and Fig. 8 we can see both the translational and rotational kinetic energy distributions are close to the theoretical results which prove the system has reached the thermal equilibrium condition.

After the system reaches thermal equilibrium, we used another 1ns to measure the time correlation function $\left\langle\vec{u}(0)\cdot\vec{u}(t)\right\rangle$. The result is shown in Fig. 9.

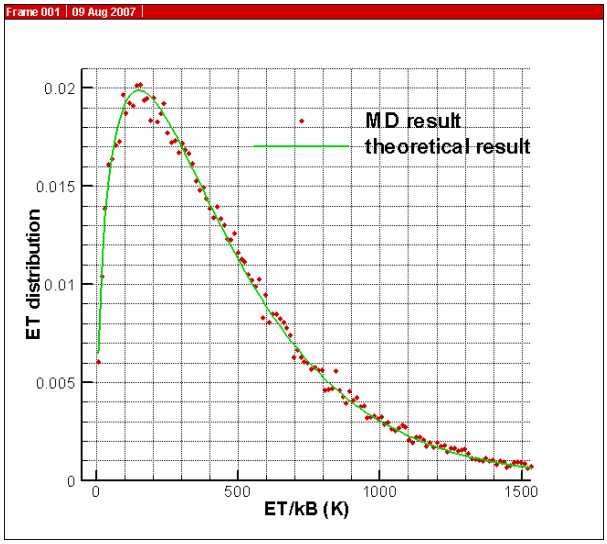

Fig. 7 Translational kinetic energy distribution

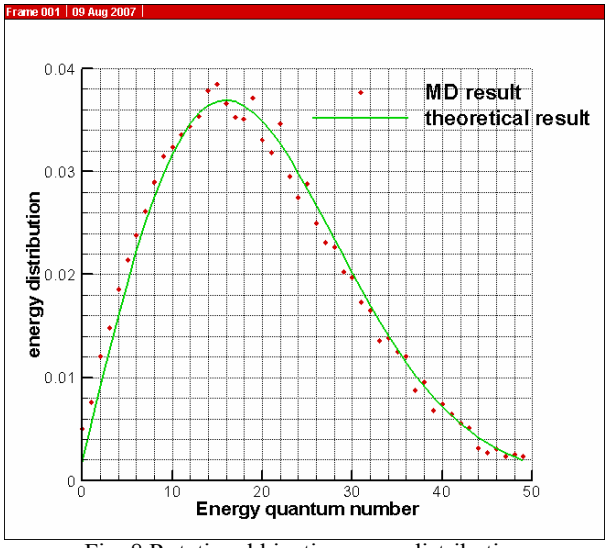

Fig. 8 Rotational kinetic energy distribution

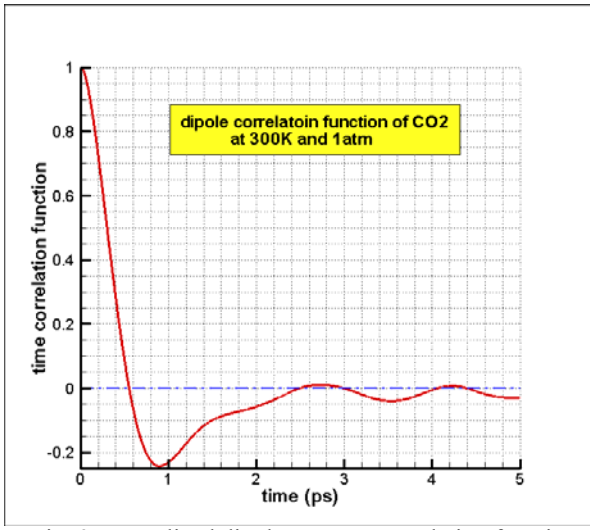

Fig. 9 Normalized dipole moment correlation function

The absorption band corresponding to Fig. 9 is the parallel band between the first excited states of the symmetric stretch and the first excited states of the asymmetric stretch mode.

The negative region in Fig. 9 indicates that it is possible the molecule swings its dipole moment to a direction opposite to which it had at t = 0. This phenomenon is also found in Gordon's paper [11]. The difference is that Gordon got the dipole correlation function by experiments.

The normalized absorption line shape is the Fourier transform of the correlation function, and the result is shown in Fig. 10.

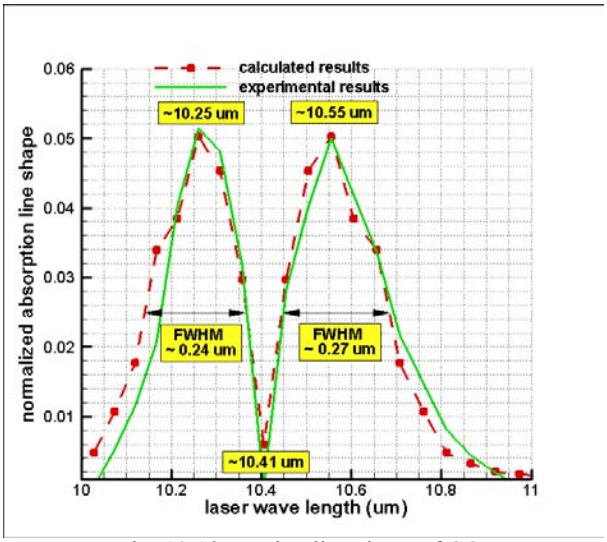

Fig. 10 Absorption line shape of CO_2

In Fig. 10, we can see two resonant wavelengths at about 10.55 μm and 10.25 μm which correspond to R branch and P branch absorption, respectively. If the laser frequency is very close to the vibration band center frequency, i.e. 10.4 μm, it has a very small absorption coefficient since this kind of transition is quantum mechanically forbidden. The absorption coefficient decreases rapidly when the laser wavelength deviates from its resonance frequency. The full width at half maximum (FWHM) of the absorption band shown in Fig. 10 is about 0.27 μm and 0.24 μm corresponding to P branch and R branch, respectively. These results are close to the experimental results [17]. The results will be improved if we use a larger t in calculating the time correlation function $\langle \bar{u}(0) \cdot \bar{u}(t) \rangle$.

The results of Fig. 10 tell us the relative absorption coefficient at a certain range of laser wavelengths. To determine the absolute value of the absorption coefficient, we need to know the wave function of the CO_2 vibration modes. This involves solving the many body Schrödinger equation and is currently under research.

CONCLUSIONS

Quantum effects must be considered in both gas thermal properties calculations and laser-gas interaction calculations. To consider the quantum effects, the ab initio MD model is used. The most critical problem in ab initio MD is the calculation of intra-molecular potential energy.

The intra-molecular potential energy of CO_2 molecules is determined by solving the many electron Schrödinger equation. This information is used in the calculation of the CO_2 vibration spectrum. We show that, at room temperature or higher, both the translational and rotational motions of CO_2 molecules can be approximated as motions of classical bodies. However, the classical approximation of vibration motion is not valid if the temperature is lower than 10^4K. On the other hand, quantum effects must be included to get the right value of CO_2 gas heat capacity. The calculated CO_2 vibration spectrum and heat capacity are close to the experimental results which verify the correctness of the potential calculated from the ab initio method.

The absorption coefficient of CO_2 gas can be calculated from its time correlation functions of the transition dipole moment. The normalized absorption line shape tells us the resonant laser wavelengths and FWHM of the CO_2 gas absorption band at 300K and 1atm.

Using a similar method described above, we expect this model is able to calculate thermal dynamics properties and laser absorption coefficient of other molecules at different temperatures and pressures.

ACKNOWLEDGMENT

This work was supported by Office of Navy Research through the Multidisciplinary University Research Initiative (MURI) program and by National Science Foundation under Grant No. 0423233.

REFERENCES

[1] Reinhard, D., 2001, Diamond Thin Films Handbook. Marcel Dekker Incorporated, New York, NY, USA.

[2] Voevodin, A.A., Donley, M.S., Zabinski, J.S., 1997, "Pulsed Laser Deposition of Diamond-Like Carbon Wear Protective Coatings: A Review," Surface and Coatings Technology, **92** (1), pp. 42-49(8).

[3] Voevodin, A.A., Donley, M.S., 1996, "Preparation of Amorphous Diamond-like Carbon by Pulsed Laser Deposition: A Critical Review," Surface and Coatings Technology, **82** (3), pp. 199-213.

[4] Roy, R., Gedevanishvili, S., Breval, E., Mistry, P., and Turchan, M., 2000, "Crystallinity Destruction in Metals by Multiple Pulsed Lasers of Different Frequency," Mater. Lett. **46**(1), pp. 30-34.

[5] Mistry, P., Turchan M., Roy, R., Gedevanishvili, S., and Breval, E., 1999, "Deep Surface Transformation And Cladding of Net Shape Commercial Steel Parts by Simultaneous Multiple Pulsed Laser Radiation," Mater. Res. Innov. **3**(1), pp. 24 – 29.

[6] Mistry, P., Turchan M. C., Granse, G. O., and Baurmann, T., 1997, "New Rapid Diamond Synthesis Technique using Multiplexed Pulsed Lasers in Laboratory Ambients," Mater. Res. Innov. **1**(3), pp. 149 – 156.

[7] Badzian, A., Weiss, B. L., Roy, R., Badzian, T., Drawl, W., Mistry, P., and Turchan, M. C., 1997, "Electron Field Emission from Diamond Grown by Laser QQC Process," The 1997 10th International Vacuum Microelectronics Conference, IVMC'97; Kyongju; South Korea; 17-21 Aug. 1997, pp. 546-550.

[8] Roy, R., Badzian, A., Breval, E., Badzian, T., Mistry, P., and Turchan, M. C., 2000, "Simultaneous Multiple Pulsed Laser (SMPL) Induced Transformations in ZrO_2 Ceramics," J Mater. Chem. **10**(10), pp. 2236-2237.

[9] Peelamedu, R., Badzian, A., Roy, R., and Martukanitz, R. P., 2004, "Sintering of Zirconia Nanopowder by Microwave-Laser Hybrid Process," J. Am. Ceram. Soc., **87**(9), pp. 1806–1809.

[10] Konov1, V. I., Prokhorov1, A. M., Uglov1, S. A., Bolshakov1, A. P., Leontiev1, I. A., Dausinger, F., Hügel, H., Angstenberger, B., Sepold, G., and Metev, S., 1998, "CO_2 Laser-Induced Plasma CVD Synthesis of Diamond," Appl. Phys. A, **66**, pp. 575–578.

[11] Gordon, R, 1965, "Molecular Motion in Infrared and Raman Spectra", J. Chem. Phys., 43, pp. 1307-1312.

[12] McQuarrie, D. A., 2000, "Statistical Mechanics", University Science Books, pp. 467-476.

[13] Born, M. and Oppenheimer, R., 1927, "Quantum Theory of Molecules", Annalen der Physik, 84, pp. 457-484.

[14] Makov, G. and Payne, M. C., 1995, "Periodic boundary conditions in ab initio calculations", Phys. Rev. B, 51, pp. 4014-4022.

[15] Goldberg L., Mohler, O. C., McMath, R. R. and Pierce, A. K., 1949, "Carbon dioxide in the infra-red solar spectrum", Phys. Rev., 76, pp. 1848-1858.

[16] Taylor, R. L., Bitterman, S., 1969, "Survey of vibrational relaxation data for processes important in the CO2-N2 laser system", Rev. of Mod. Phys., 41, pp. 26-46.

[17] The HITRAN data base in Harvard University, http://cfa-www.harvard.edu/HITRAN/